SUPPLEMENTARY MATERIAL VOLCANICA

Supplementary Material for:

Effects of vent-sourced external water on volcanic column height and collapse

Edgar L. Carrillo *[αβγ], Kristen E. Fauria[β], Tushar Mittal[δ], and Larry G. Mastin[ε]

[α] Department of Physics, Fisk University, Nashville, TN 37208, USA.
[β] Department of Earth and Environmental Science, Vanderbilt University, Nashville, TN 37235, USA.
[γ] Department of Earth Science, University of Oregon, Eugene, OR 97403, USA.
[δ] Department of Geoscience, Pennsylvania State University, University Park, PA 16802, USA.
[ε] U.S. Geological Survey, Cascades Volcano Observatory, Vancouver, WA 98683, USA.

This supplementary material accompanies the article:

> Carrillo, E., Fauria, K., Mittal, T. and Mastin, L. (2026) "Effects of external water on volcanic column height and collapse", *Volcanica, 9*(1), pp. 175–186. DOI: 10.30909/vol/ycra8102.

Carrillo et al. (2026) should be cited if this material is used independently of the article.

S1 Dry equivalent mass flux

This study aims to understand how external water impacts column height and collapse for an eruption of a given mass flux or mass eruption rate (MER). A complicating factor is that the addition of external water, by definition, increases the eruption mass flux. By adding external water to an eruption column, more mass is present in the column than in the dry case.

We follow the convention of Mastin [2007] and Koyaguchi and Woods [1996] and consider the relevant MER the dry equivalent mass flux. The dry equivalent mass flux is the MER without any external water added and is defined as

$$M_d = \pi r^2 \rho_{dry} u \tag{S1}$$

where r is the initial vent radius, ρ_{dry} is the dry mixture density at the vent, including gas and magma, and u is the vent exit velocity.

The addition of external water at the vent affects the mixture density. The total mass flux with external water, M_T, is defined as

$$M_T = \pi r^2 \rho_{mix} u \tag{S2}$$

where ρ_{mix} is the wet mixture (liquid water, vapor, and magma) density. To examine the impact of increasing external water, we define the parameter $w = 1 - m_v - m_m$, where $m_v = m_g + m_0$, m_0 is initial volatile content, and m_g is the vaporized component of the external water. This dimensionless parameter represents the mass fraction of external water in the mixture. Here, m_v = vapor mass/total mass is the initial mass fraction of vapor, and m_m = magma mass/total mass is the initial mass fraction of magma. Thus the relation of M_d (Equation S1) and M_T (Equation S2) is

$$M_T(1 - w) = M_d. \tag{S3}$$

To be clear, we use M_d (Equation S3) to represent the MER and compare our results with varying amounts of external water.

S2 Limitations of 1D models in capturing near-vent water entrainment

As noted in Section 2 of the main text, the impact of external water on column stability depends significantly on the conditions of its introduction. As external water is introduced and thermally equilibrates with the mixture, the overall density of the erupting jet decreases. To maintain a constant mass flux, either the jet velocity or vent diameter must increase.

These adjustments have competing effects on entrainment and column stability. An increase in velocity enhances entrainment, stabilizing near-collapsing jets, while an increase in vent diameter reduces entrainment efficiency relative to mass flux, thereby promoting instability. It is, therefore, critical to consider the physical rationale behind the chosen model inputs.

We assume an idealized jet in which magma and gas flow is initially restricted at a near-vent constriction (see Figure S1a). Above this constriction, the vent expands, and the mixture undergoes rapid decompression to atmospheric pressure as it accelerates. The model domain begins at the point within or just above the crater, where the erupting mixture has equilibrated to atmospheric pressure.

If external water enters the jet at atmospheric pressure along its boundary (see Figure S1b), the jet will widen due to the added mass, and the entrained water (having zero initial upward momentum) will act to decelerate the jet. This velocity reduction can be estimated using the conservation of momentum:

$$M_T u = M_d u_{dry} + M_w u_w \tag{S4}$$

* elcar@uoregon.edu

Editor: S. Scollo & A. H. Graettinger | Typesetter: J. Farquharson

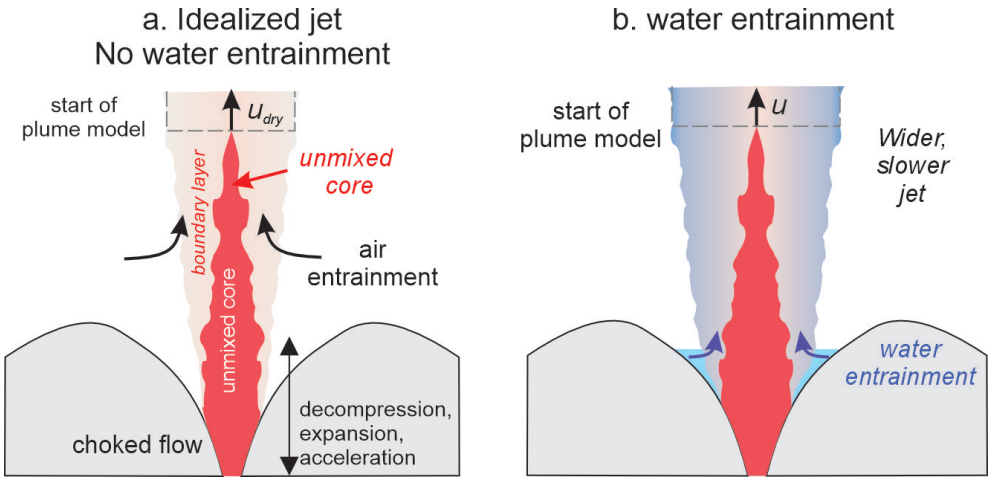

Figure S1: Schematic, adapted from Figure 3 of Mastin et al. [2024], illustrating the impact of external water addition on jet velocity and entrainment. (a) An idealized dry jet undergoes decompression and acceleration as it expands from a near-vent constriction to atmospheric pressure. (b) When external water is entrained at atmospheric pressure along the jet boundary, the jet expands laterally, increasing its diameter while reducing its velocity due to momentum conservation

where M_T, M_d, and M_w are the mass fluxes of the total mixture, the dry magma+gas mixture, and the external water, respectively. The terms u, u_{dry}, and u_w are the upward velocities of the wet mixture, the dry jet, and the entrained water, respectively, before mixing. Assuming $u_w = 0$ and substituting $M_d = M_T(1-w)$ and $M_w = M_T w$ into Equation S4, we obtain:

$$u = u_{dry}(1-w). \tag{S5}$$

This relation indicates that adding external water at the vent reduces the jet velocity in proportion to the added water fraction. To maintain a constant mass eruption rate, we adjust the vent diameter accordingly, which leads to a shift in the critical collapse condition when using the wet velocity (u in Equation S5). This effect is illustrated in Figure S2b.

For the results presented in the main text (Figures 2, 3, and 4 in main text), we model only the aerial phase of the plume and do not explicitly resolve near-vent interactions between the jet and external water. As such, the mass eruption rate, jet radius, and velocity are treated as "effective" properties, simplifying the complex entrainment processes that occur at the vent. These processes include interactions between eruptive jets and water plumes generated by pyroclastic flows, steam explosions from ballistic material impacting the water surface, and various combinations of these mechanisms.

We note that the reduced "wet" velocity is *not* applied in our simulations. Instead, we hold the mass eruption rate constant and adjust the vent diameter accordingly with a constant "dry" velocity. The velocity reduction discussed above is included only to highlight the complex interplay between momentum conservation and entrainment when external water is added. Future work incorporating more detailed near-vent dynamics, such as that explored in Rowell et al. [2022], would be required to fully capture these effects.

Due to the inherent limitations of a 1D model, resolving these detailed entrainment dynamics is beyond the scope of this study. Instead, we focus on parameterizing the effective properties of the jet, which also justifies the temperature adjustments applied at the model input. However, both observations and physical constraints suggest that vent widening occurs at larger eruption rates, reinforcing our focus on varying vent radius as a function of mass eruption rate in this study.

S3 Bulk mixture dynamics in volcanic columns

S3.1 Effects of external water on bulk mixture density

We plot the initial mixture density as a function of external water content ($w = \frac{\text{external water mass}}{\text{total mixture mass}}$) for the simulation results at $T = 900$ °C, $u = 100$ m s^{-1} (magma temperature and vent exit velocity, respectively), and constant values from Table 1 in the main text (Figure S3). Additionally, we show the compositional evolution of the mixture as external water is added (Figure S3 inset). To understand why external water affects the column collapse condition, we consider how the incorporation of external water affects the average density, vapor and liquid phase fraction, and temperature of the eruptive mixture. First, adding external water to a magmatic mixture lowers its bulk density. The degree to which water lowers the bulk density depends on the phase of the water (vapor vs. liquid water) and, thus, the mixture temperature (Figure 1, Equation S6). Using the assumption that thermal energy is conserved and that thermal equilibrium is reached during the mixing process, we calculate that mixture temperatures of ≈100 °C are reached once ≈25 wt.% of water is added (Section 1.2, Figure S3). As a result, the magma temperature drops by an amount proportional to the thermal energy transfer to the external water. We find that with a mass fraction of external water of ≈0.25, the mixture temperatures ~100 °C are reached, and we start getting an increasing amount of liquid water (which is denser than air) in the mixture with a corresponding increase in the mixture density.

S3.2 Calculating mixture density

The density of the column bulk mixture (ρ_{mix}) can be derived from the mixture volume (V_{mix}), which is the total volume of

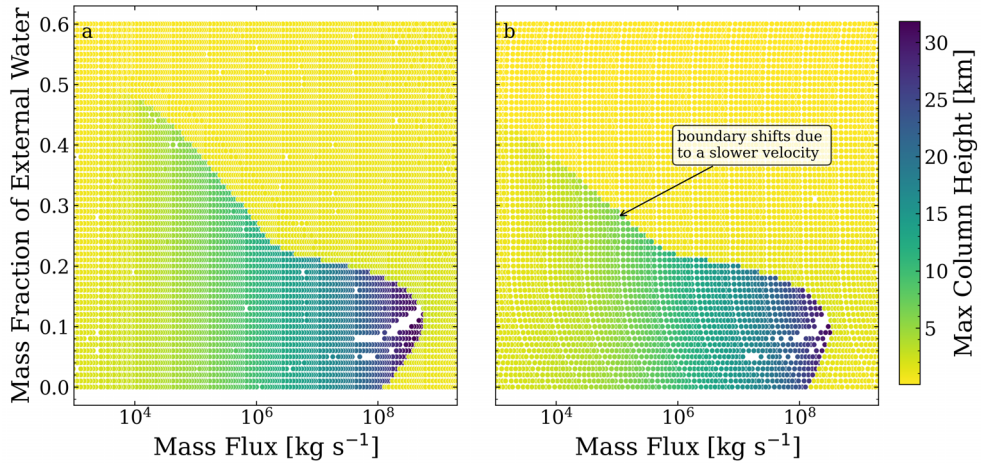

Figure S2: The impact of external water on jet velocity results in a reduced initial jet speed. This reduction, in turn, influences the stability of the column, shifting the collapse condition slightly to the left. Panel (a) shows the results from Figure 2e in the main text, while panel (b) uses the same inputs as panel (a) but includes a "wet" velocity (Equation S5). These results were produced with an earlier version of `Plumeria`, prior to recent updates that improved numerical, thermodynamic, and input-handling behavior; the updated version used for the main-text figures yields the same physical trends.

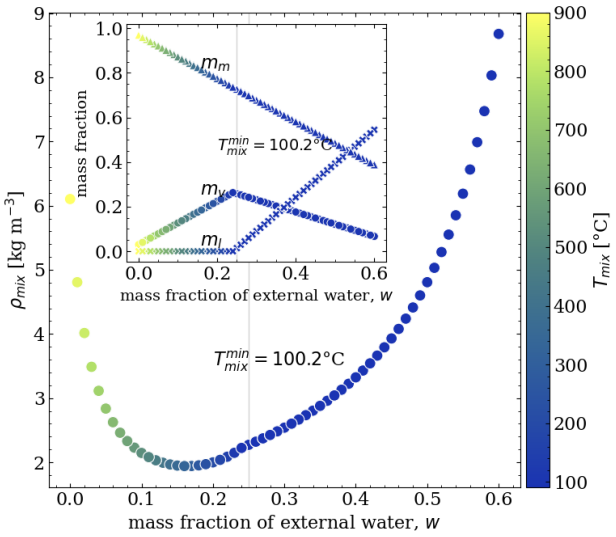

Figure S3: Effect of varying mass fraction of external water, w, on mixture density (ρ_m, kg m^{-3}) changes at the vent for varying mass fraction of external water (w). The inset plot shows the changing composition of the mixture (mass fraction of; magma, m_m, vapor, m_v, and liquid, m_l) as external water is added. The minimum temperature from all runs, with $T = 900$ °C and $u = 100$ m s^{-1}, that the mixture reaches (T^{min}_{mix},°C) is shown for reference. The varying mixture temperature, (T_{mix}, °C) is also shown.

all components:

$$V_{mix} = \sum_{i=1}^{N} X_i V_i \quad \text{where} \quad \sum_{i=1}^{N} X_i = 1.$$

Here, V_i represents the volume of each component. Using the density relation, $\rho = \frac{\text{mass}}{\text{volume}}$, the column bulk mixture density is

$$\rho = \left[\underbrace{\frac{(m_a R_a + m_v R_w) T_{mix}}{P}}_{\text{vapor + air}} + \underbrace{\frac{m_l}{\rho_l}}_{\text{liquid}} + \underbrace{\frac{m_m}{\rho_m}}_{\text{magma (solids)}} + \underbrace{\frac{m_i}{\rho_i}}_{\text{ice}} \right]^{-1}, \tag{S6}$$

where T_{mix} represents the bulk mixture temperature. The variables m_a, m_v, m_l, and m_i denote the mass fractions of air, gas (assumed to be vapor only), liquid water, and ice, respectively. The constants R_a and R_w correspond to air and water vapor, respectively. Meanwhile, P is the ambient pressure, ρ_l is the density of liquid water, ρ_m is the density of magma (DRE), and ρ_i is the density of ice. When external water is present, the liquid water can undergo full, partial, or no vaporization. Thus, the resulting mixture's density depends on the added water's mass fraction, as it affects the balance between ice, vapor, and liquid (Appendix B5 in Mastin [2007]). This balance is influenced by the temperature of the mixture.

S3.3 Temperature dependence of mixture density

From Figure 1 we see that the minimum mixture density is not when mixture temperature reaches a minimum, that is $\frac{d\rho_{mix}}{dT_{mix}} \neq 0$. We can see this is true analytically since

$$\frac{\partial \rho_{mix}^{-1}}{\partial T_{mix}} = \frac{\partial}{\partial T_{mix}} \left(\frac{m_v R_w T_{mix}}{P} + \frac{m_l}{\rho_l} + \frac{m_m}{\rho_m} \right) = \frac{m_v R_w}{P} \tag{S7}$$

and $\rho_{mix} = (\rho_{mix}^{-1})^{-1}$, so

$$\frac{d\rho_{mix}}{dT_{mix}} = -(\rho_{mix})^{-2}\left(\frac{m_v R_w}{P}\right). \tag{S8}$$

Because m_v, R_w, P, and ρ_{mix} are all positive physical quantities, the derivative is always negative and never zero (i.e. $\frac{\partial \rho_{mix}}{\partial T_{mix}} \neq 0$). Thus, Equation S7 and Equation S8 confirm that mixture density cannot reach its minimum value through temperature alone; it also depends on the distribution of water between vapor and liquid phases. Physically, the minimum density occurs at an intermediate temperature where most of the water is vapor, but before liquid water dominates the mixture. As soon as liquid water becomes significant, density increases sharply, producing the characteristic minimum seen in Figure S3.

This critical point corresponds to the "optimal" magma–water mixing ratio identified by Wohletz [1986]. At this ratio, the magmatic enthalpy is just sufficient to vaporize the added water. If less water is present, excess enthalpy remains in the solids; if more water is present, insufficient enthalpy is available to fully vaporize it, resulting in liquid water and a higher bulk density.

S3.4 Critical density and buoyancy conditions

The critical mixture density necessary for buoyancy is attained when $\rho \approx \rho_{air}$. At this critical density, the mass fractions of ice and magma/solids can be neglected, leading to the condition $\xi = \xi_{crit}$ (refer to Appendix A of Koyaguchi and Suzuki [2018]).

S3.5 Initial density of wet and dry mixtures

Equation S6 describes the general formulation for bulk mixture density and can be applied at any point along the column, including the convective region. When analyzing the mixture density at the vent, we consider the initial vapor content present as volatiles in the magma, denoted as m_0, while neglecting air (m_a). The mixture density at the source, where no external water is introduced, is thus

$$\rho_{dry} = \left[\underbrace{\frac{m_0 R_w T_{dry}}{P}}_{\text{vapor}} + \underbrace{\frac{m_m}{\rho_m}}_{\text{magma (solids)}}\right]^{-1}. \tag{S9}$$

where T_{dry} is the initial mixture temperature for dry eruptions. When external water is added, the density of the initial mixture depends on the mass fraction of the added water, as it affects the balance between vapor and liquid (no ice for the initial mixture) (Appendix B1 in Mastin [2007]). This balance is influenced by the initial temperature of the mixture. Therefore, the initial wet mixture density (the bulk mixture density when external water is added) will be generally

$$\rho_{wet} = \left[\underbrace{\frac{m_v R_w T_{mix}}{P}}_{\text{vapor}} + \underbrace{\frac{m_l}{\rho_l}}_{\text{liquid}} + \underbrace{\frac{m_m}{\rho_m}}_{\text{magma (solids)}}\right]^{-1}. \tag{S10}$$

In this case, m_v is the total vapor in the mixture, including initial volatile content. Equation S9 follows from Equation S10 for $w = 0$.

S3.6 Heat balance and mixture temperature

The mass fraction of erupted material (magma+gas) is given by $\xi = m_v + m_m$, where the mass fraction of ice is not considered. This mass fraction can be used to calculate the mixture temperature from a heat balance. We assume heat capacity is constant with temperature, $h = C_p T$ where C_p is the specific heat. The specific heat capacities are denoted as follows: $C_{p,m}$ for magma (erupted solids), $C_{p,w}$ for liquid water, $C_{p,a}$ for air, $C_{p,v}$ for vapor, and $C_{p,m}$ for the mixture. Additionally, L_v indicates the latent heat associated with vaporization. The heat balance, utilizing the initial and final states of the mixture's internal energy, can be expressed as

$$h_i = \underbrace{\xi C_{p,m} T_m}_{\text{erupted material}} + \underbrace{m_l C_{p,w} T_w}_{\text{liquid water}} + \underbrace{(1-\xi-m_l) C_{p,a} T_a}_{\text{air}}, \tag{S11}$$

where T_m is the magma temperature, T_w is liquid water temperature, and T_a is ambient air temperature.

$$h_f = \underbrace{\left(\xi C_{p,m} + m_l C_{p,w} + (1-\xi-m_l) C_{p,a}\right) T_{mix}}_{\text{mixture}} + \underbrace{m_v (C_{p,v} T_{mix} + L_v)}_{\text{vaporized component}}. \tag{S12}$$

Equating Equation S11 and Equation S12, the mixture temperature is:

$$T_{mix} = \frac{\xi C_{p,m} T_m + m_l C_{p,w} T_w + (1-\xi-m_l) C_{p,a} T_a - m_v L_v}{\xi C_{p,m} + m_l C_{p,w} + (1-\xi-m_l) C_{p,a} + m_v C_{p,v}}. \tag{S13}$$

We note that for the *initial* mixture temperature, there is no air in the mixture ($1-\xi-w=0$) thus Equation S13 reduces to

$$T_{mix}^{init} = \frac{\xi C_{p,m} T_m + m_l C_{p,w} T_w - m_v L_v}{\xi C_{p,m} + m_l C_{p,w} + m_v C_{p,v}}. \tag{S14}$$

When the mass fraction of external water is low (i.e., $m_l = 0$), complete vaporization of water can occur. In this scenario, the initial mixture temperature (from Equation S14) primarily decreases proportionally to heat loss from vaporization, $T_{mix}^{init} \propto T_m - m_v L_v$. The overall mixture temperature will remain above the boiling point, and the temperature change can be significant relative to T_m. Additionally, the bulk mixture density can reach critical density. Conversely, when there is a significant mass fraction of external water (i.e., $m_l > 0$), the temperature will change drastically. That is, T_{mix} must be at or below the boiling point of water, so $T_{mix} \ll T_m$ because the amount of added water is great enough that there is insufficient enthalpy in the magma to boil all of the water.

S4 Adjusting vent diameter to keep mass flux constant

Given an initial radius for a circular vent (r_d, m), vent exit velocity (u, m s^{-1}), and mixture (magma+gas) density (ρ_{dry}, kg m^{-3}), let M_d (from Equation S1) be an initial dry mass eruption rate (mass flux, kg s^{-1}). When external water

is added to the mixture at the vent (with the mass fraction of the added water denoted by w), the mixture's density at the vent changes to ρ_{mix}. This total density accounts for both the mixture and the added water. The mass flux of the wet eruption is defined as

$$M_w = \pi r_w^2 \rho_{mix} u, \tag{S15}$$

where we assume that the velocity remains constant for both wet and dry eruptions. Since the mass fraction of water in the mixture is w, the mass fraction of magma in the mixture is $1 - w$ such that $w + (1 - w) = 1$. We, therefore, state that

$$M_T = \pi r_w^2 \rho_{mix} u(w + (1 - w)) \tag{S16a}$$

$$M_T = \underbrace{\pi r_w^2 \rho_{mix} u w}_{M_w} + \underbrace{\pi r_w^2 \rho_{mix} u(1 - w)}_{M_{m,g}} \tag{S16b}$$

The mass flux from external water added is M_w, and the mass flux from magma and gas is $M_{m,g}$. In this case, $M_T \neq M_d$ for $w > 0$. To examine the effects of adding external water to a dry eruption, we relate $M_{m,g}$ and M_d where $w > 0$ and the initial vent velocity does not change. To do this, we let $M_d = M_{m,g}$, u_0 be a constant vent exit velocity, and let vent radius vary such that

$$M_d = M_{m,g} \tag{S17a}$$

$$\pi r_d^2 \rho_{dry} u = \pi r_w^2 \rho_{mix} u(1 - w) \tag{S17b}$$

$$r_w = r_d \left(\frac{\rho_{dry}}{\rho_{mix}(1 - w)} \right)^{\frac{1}{2}} \tag{S17c}$$

Thus, enforcing $M_{m,g} = M_d$ (using Eqs. S15 and S16) at constant exit velocity yields Equation S17. Equation S17c then defines the vent radius required to maintain a constant magma-plus-gas mass flux.

S5 Effects of external water on column behavior: Four regions of impact

S5.1 Region 1

Region 1 corresponds to low MER values ($\sim 10^4$ kg s^{-1}) and the full range of external water content (0 – 60 wt.%), where column heights are only slightly suppressed or enhanced compared to dry eruptions (Figure S4). Figure S4 illustrates how external water affects the evolution of column velocity, mixture temperature, and mixture density for MER values of $\sim 10^4$ kg s^{-1} and varying external water contents.

The minimal change in column height observed in Region 1 (from Figure 3a in the main text) results from the limited thermal energy added by the external water. The energy transfer mechanism between the magma-water mixture and the surrounding air is governed by convective turbulence as air is engulfed into eddies on the jet margin. At the vent, thermal energy from the magma is used to heat and vaporize the external water, but the latent heat consumed during vaporization is largely recovered during condensation in the rising column [Woods 1993]. This recovery of latent heat by condensation mitigates the overall impact of external water on column dynamics, leading to minimal changes in column height.

To quantify this, we define the thermal energy ratio of the mixture as

$$H_{mix} = \frac{C_m T_m}{C_w T_w} w \tag{S18}$$

where C_m is the heat capacity of magma, C_w is the heat capacity of water, T_m is the initial magmatic temperature, T_w is the initial temperature of external water, and w is the mass fraction of external water.

For typical conditions where the external water temperature is close to atmospheric values, and the heat capacities of magma and water are approximately 1000 and 4000 J kg^{-1} K^{-1}, respectively, Equation S18 shows that magmatic enthalpy dominates. With an initial magmatic temperature of 900°C, the external water contributes minimally to the initial thermal energy in the eruption column. This is because most of the energy from the magma is absorbed by heating the water and driving vaporization, but as the plume rises and cools, the condensation of the vapor releases this latent heat back into the plume, balancing much of the energy lost at the vent. Thus, the overall minimal impact in Region 1 is a consequence of latent heat recovery during condensation, which offsets the energy lost to vaporization at the vent.

Generally, the results for Region 1 agree with results from empirical models such as Eq. 5.1 of Sparks et al. [1997].

S5.2 Region 2

In Region 2 from Figure 2 in the main text, the wet column height is significantly lower, by $\approx 10 - 30$ km, than the dry column height at the equivalent mass flux because the wet columns collapse. For example, Figure 3b-g in the main text shows that the modeled maximum heights of dry (0 wt.% water) and wet (30 wt.% water) columns are 18 and 1 km, respectively.

Column height decreases significantly in Region 2 because a large amount of external water makes the initial mixture too

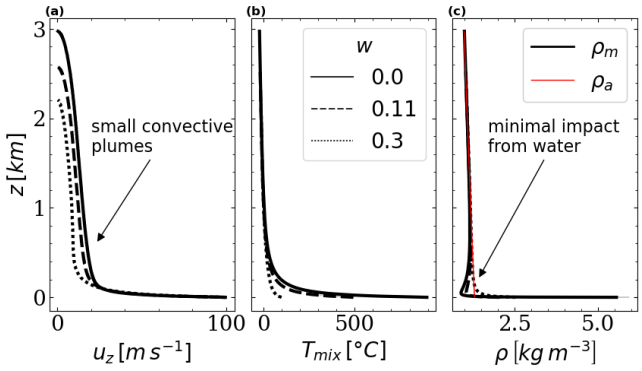

Figure S4: Results from individual `Plumeria` simulations where the initial mass eruption rate is $\sim 10^4$ kg s^{-1} (Region 1 from Figure 3a in the main text). (a-c) The evolution of upward velocity (u_z, m s^{-1}), mixture temperature (T_{mix},°C), and mixture density (ρ_m, kg m^{-1}) above the vent is shown. We show ambient air (ρ_a, kg m^{-1}) density as a reference density. Here, z denotes height above the vent, such that these panels show the vertical evolution of plume properties rather than a single plume-height metric.

dense and too cold to become buoyant. Figure 3c from the main text shows that in the dry case, the initial temperature is close to the magmatic temperature, while in the case where 30 wt.% external water is added, the temperature is close to 100°C (as expected from Figure 1). As the mixture temperature approaches the boiling point, water exists in both vapor and liquid states within the column. The liquid water is denser than ambient air, thus reducing the column buoyancy. Furthermore, since the column's thermal energy is used up to heat/vaporize external water, the entrained air by the column is not heated and expanded as effectively to form a tall buoyant column. Therefore, relative to the dry case, we see a decrease in column height because external water heating consumes a substantial portion of the thermal energy available, preventing the column from becoming buoyant. The mixture thus forms a wet collapsing column.

S5.3 Region 3

For large eruptions (MER values much greater than 10^8 kg s^{-1}), adding external water to the mixture has a relatively minor effect on the maximum column height. In Region 3 (as shown in Figure 3a of the main text), the heights are low (approximately less than 5 km), and in this region, no columns become buoyant (see Figure S5a). Instead, the heights observed in Region 3 reflect the maximum height of a negatively buoyant jet or fountain. From Equation S20 we can see that H_{mmt} increases as the mixture density decreases while keeping velocity constant. Figure S5c illustrates that the density of the wet mixture is lower than that of the dry mixture. Consequently, the jet height of wet eruptions will be greater than that of dry eruptions. Regardless of how much external water is added, the mass fluxes are sufficiently high in Region 3 that air entrainment does not induce buoyancy in the column.

We find that external water increases the column height in Region 3 on the order of a kilometer. We do not consider this slight increase to be physically significant. Instead, the height increase is an outcome of the initial model setup. Specifically, the initial magma and external water mixture is ejected at a constant velocity regardless of the amount of external water added. That is, the external water is effectively instantaneously accelerated to the initial velocity of the magma at the vent. Consequently, in Region 3, maximum column height is governed by mixture density. Figure S5 shows that columns with external water have lower initial densities and, therefore, can move further vertically.

S5.4 Region 4

In Region 4 from Figure 2 in the main text, adding external water increased column heights up to 40 km, relative to dry eruptions that collapse. MER values are large ($\gtrsim 10^8$ kg s^{-1}) in Region 4 and include external water content values less than 25 ± 4 wt.%.

We find that adding a small to moderate amount of external water lowers the initial mixture density substantially without cooling the mixture below the boiling temperature. The external water is thus vaporized, allowing the column to become buoyant with a smaller amount of air entrainment in the jet phase of the column compared to the dry case (Figure 3g from main text). Region 4 is thus a "sweet spot" where external water decreases initial mixture density and increases column height by making an otherwise collapsing column buoyant. Like the other regions, the specific MER and w values that define Region 4 also depend on the initial speed at the vent and magma temperature since the initial velocity controls entrainment while the magma temperature controls the available thermal energy. Overall, we find that the reduced density of external water has a greater effect at high initial MER values ($\gtrsim 10^8$ kg s^{-1}) because the air entrainment, which enhances buoyancy, is less effective in eruptions with high MERs and large vent diameters.

S6 Effect of ice formation in wet volcanic column dynamics

We run simulations using `Plumeria` where ice is not allowed to form and compare the results to those when ice is allowed to form. To understand the effects of ice formation, we vary external water content (w; 0–60 wt.%), mass eruption rate (M_d; $10^2 - 10^{12}$ kg s^{-1}), and relative humidity (ϕ; 0%, 50%, 100%). All other parameters are held constant (values from Table 1 in the main text). Results are shown in Figure S6. There is a marginal increase in plume height between the scenario in which ice is allowed to form and when it is not. Furthermore, moisture in the atmosphere has a negligible effect on ice formation. We note that increased humidity does generally increase plume height for the low mass flux case ($\lessapprox 10^6$ kg s^{-1}) and agrees with the results from Woods [1993] and Koyaguchi and Woods [1996]. Generally, ice formation does not enhance or suppress the effect of external water on column dynamics. This is partly because the initial thermal energy of the magma dominates the column's enthalpy (Equation S18).

S7 Theoretical background on column height and mass eruption rate

Physics-based theory and non-dimensional analysis suggest that maximum plume height (H, km) scales with buoyancy flux and thus volumetric discharge rate (Q, km^3 s^{-1}) such that $H \propto Q^{0.25}$ [Morton et al. 1956; Sparks et al. 1997]. Sparks et al. [1997] suggested the empirical relation

$$H = 0.22\,\dot{M}^{0.259}, \tag{S19}$$

where $\dot{M}$ is eruption discharge rate (kg s^{-1}) (converted to mass flux from volume flux using Equation 1 of Mastin [2014] (Figure 1b in the main text). Observations of modern eruptions align with these scalings relatively well [Mastin et al. 2009; Aubry et al. 2021]. Consequently, empirical scaling relations are commonly used to estimate mass flux by inverting plume height [Sparks et al. 1997; Mastin et al. 2009; Degruyter and Bonadonna 2012]. Such plume heights can often be measured using remote sensing techniques [Gupta et al. 2022].

Equation S19 is not universally applicable for volcanic columns as real eruption columns do not always become buoyant and rise kilometers into the atmosphere (Figure 1b from the main text). At large mass fluxes, eruption columns

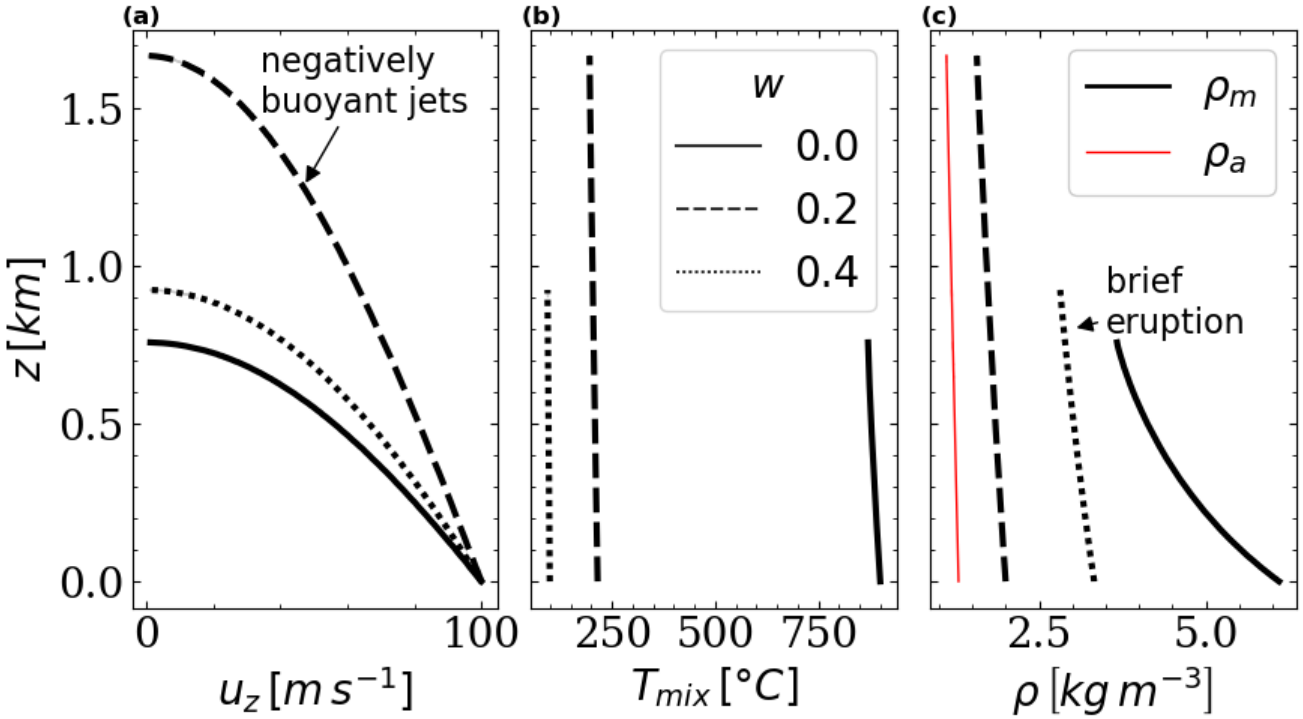

Figure S5: Results from individual `Plumeria` simulations where the initial mass eruption rate is $\sim 10^9$ kg s^{-1} (Region 3 from Figure 3a in the main text). (a-c) The evolution of upward velocity (u_z, m s^{-1}), mixture temperature (T_{mix},°C), and mixture density (ρ_m, kg m^{-3}) above the vent is shown. We show ambient air (ρ_a, kg m^{-3}) density as a reference density. Here, z denotes height above the vent, such that these panels show the vertical evolution of plume properties rather than a single plume-height metric.

can fail to entrain and heat enough air to become buoyant and may collapse.

The condition for column collapse can also be derived from theoretical considerations. The height at which column momentum is exhausted (H_{mmt}) is given by [Suzuki and Koyaguchi 2012; Koyaguchi and Suzuki 2018]:

$$H_{mmt} \approx \rho_{mix} \frac{u^2}{g(\rho_{mix} - \rho_0)}, \tag{S20}$$

where ρ_{mix} is the bulk density of the volcanic mixture, u is the upward velocity, g is gravitational acceleration, and ρ_0 is the ambient air density. Equation S20 therefore defines the momentum-exhaustion height used to assess the onset of column collapse. In the case of dry eruptions ($w = 0$) for Region 4 (Figure 3a,e,f in main text), column collapse occurs when $\rho_{mix} > \rho_0$ as $u_z \to 0$.

For eruptions involving external water, ρ_{mix} becomes a function of temperature (T) as water is added (Section S3.5 of this supplementary file). The bulk mixture remains above the boiling point when $w < 25 \pm 4$ wt.% (w_{crit}; Figure 3g from main text), leading to a decrease in ρ_{mix} below ρ_0. When $w < w_{crit}$, buoyancy is induced before the plume's momentum is depleted.

S8 Critical mass fraction with external water

Following the framework of Koyaguchi and Suzuki [2018], we extend the derivation of the critical erupted fraction ξ_{crit} to include a third component: external water. This extension applies to the case where external water is treated as vapor; accounting for liquid phases and latent heat of vaporization would require additional terms in the enthalpy balance and is beyond the scope of this derivation.

S8.1 Setup

We first define mass fractions:

$$\begin{aligned} \xi &= \text{erupted material (magma + magmatic gas)}, \\ \omega &= \text{external water}, \\ 1-\xi-\omega &= \text{entrained air}. \end{aligned}$$

Within the erupted material, a fraction n is volcanic gas; the remainder are pyroclasts that contribute to heat capacity but not volume.

The mixture gas constant is $R_{\text{mix}} = \xi n R_g + \omega R_w + (1-\xi-\omega)R_{\text{air}}$, and the mixture temperature T is obtained from enthalpy conservation:

$$T = \frac{\xi C_{p,m} T_m + \omega C_{p,w} T_w + (1-\xi-\omega) C_{p,\text{air}} T_{\text{air}}}{\xi C_{p,m} + \omega C_{p,w} + (1-\xi-\omega) C_{p,\text{air}}}. \tag{S21}$$

S8.2 Collapse condition

At the collapse threshold, the mixture density equals ambient air density:

$$\frac{p}{R_{\text{mix}} T} = \frac{p}{R_{\text{air}} T_{\text{air}}} \quad \Longrightarrow \quad R_{\text{mix}}\, T = R_{\text{air}} T_{\text{air}}.$$

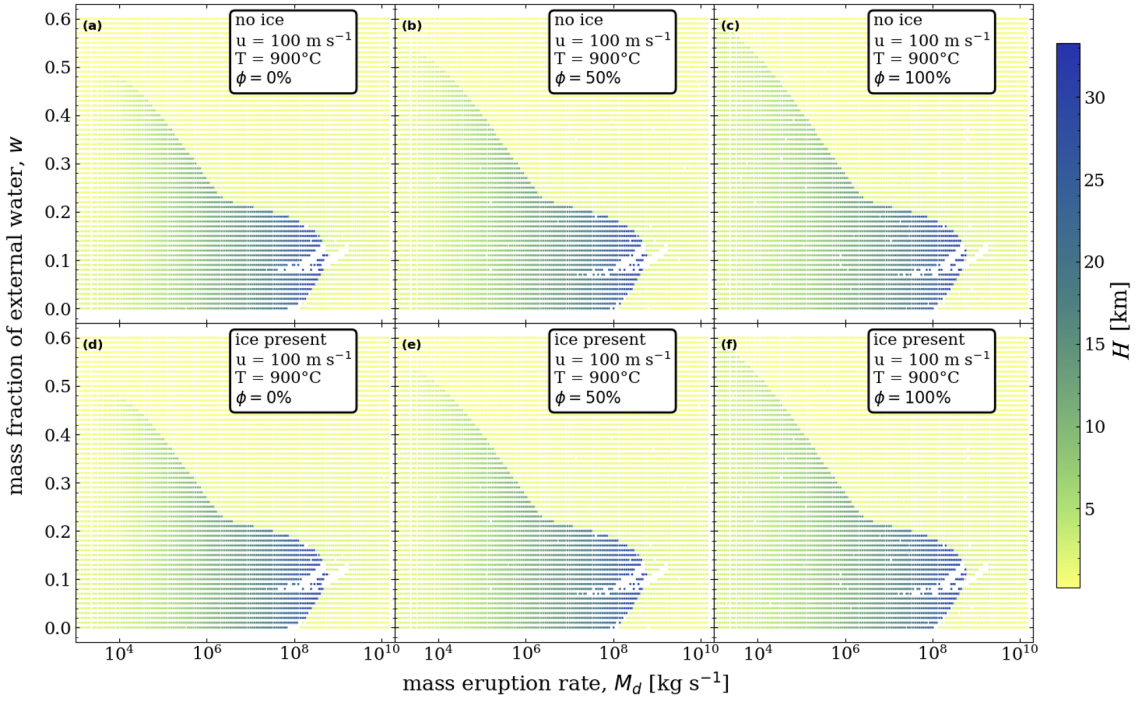

Figure S6: `Plumeria` results for maximum column height (H, km) as a function of mass fraction of external water (w) and mass eruption rate (M_d, kg s^{-1}). The results shown correspond to model run inputs from Figure 3a in the main text, with (a-c) no ice formation and (d-g) with ice formation, and relative humidity values, ϕ, of 0, 50, and 100 %. These results were produced with an earlier version of `Plumeria`, prior to recent updates that improved numerical, thermodynamic, and input-handling behavior; the updated version used for the main-text figures yields the same physical trends.

This condition reduces to a quadratic equation in ξ,

$$a\,\xi^2 + b\,\xi + c = 0, \tag{S22}$$

with coefficients

$$\begin{aligned} a &= -\left(R_{\text{air}} - nR_g\right)\left(C_{p,m}T_m - C_{p,\text{air}}T_{\text{air}}\right), \\ b &= R_{\text{air}}C_{p,m}(T_m - T_{\text{air}}) - \left(R_{\text{air}} - nR_g\right)C_{p,\text{air}}T_{\text{air}} \\ &\quad - \omega\Big[\left(R_{\text{air}} - R_w\right)\left(C_{p,m}T_m - C_{p,\text{air}}T_{\text{air}}\right) \\ &\quad + \left(R_{\text{air}} - nR_g\right)\left(C_{p,w}T_w - C_{p,\text{air}}T_{\text{air}}\right)\Big], \\ c &= \omega\Big[R_{\text{air}}C_{p,w}(T_w - T_{\text{air}}) \\ &\quad - \left(R_{\text{air}} - R_w\right)C_{p,\text{air}}T_{\text{air}}\Big] \\ &\quad - \omega^2\left(R_{\text{air}} - R_w\right)\left(C_{p,w}T_w - C_{p,\text{air}}T_{\text{air}}\right). \end{aligned} \tag{S23}$$

S8.3 Critical mass fraction

The physically admissible root, continuous with the no-water case, is

$$\xi_{\text{crit}}(\omega) = \frac{-b - \sqrt{b^2 - 4ac}}{2a}, \tag{S24}$$

subject to $0 \le \xi_{\text{crit}} \le 1 - \omega$.

S8.4 Recovery of the no-Water expression

Setting $\omega = 0$ in Equation S22 reduces $c = 0$ and recovers the expression of Koyaguchi and Suzuki [2018] (their eq. A3):

$$\xi_{\text{crit}} = \frac{R_{\text{air}}C_{p,m}(T_m - T_{\text{air}}) - C_{p,\text{air}}T_{\text{air}}(R_{\text{air}} - nR_g)}{(R_{\text{air}} - nR_g)(C_{p,m}T_m - C_{p,\text{air}}T_{\text{air}})}.$$

S9 Richardson numbers at the column collapse condition

S9.1 Richardson number formulation

The Richardson number (Ri) quantifies the balance between buoyancy and shear forces in fluid flow, critical for understanding volcanic column dynamics. It is calculated as $Ri = \frac{g'r}{u_0^2}$, where $g' = g\frac{\rho_{mix} - \rho_0}{\rho_{mix}}$ is the reduced gravity, ρ_{mix} is the mixture density, ρ_0 is the ambient air density, g is gravitational acceleration, r is the initial vent radius, and u_0 is the vent exit velocity. We also consider the modified Richardson number, $\gamma = \frac{Ri}{\alpha}$ (Eq. 2 in the main text), which depends on temperature and external water content (Figure S7a).

S9.2 Thermal Richardson number

To evaluate the role of thermal convection in column buoyancy, we define the Thermal Richardson Number (Ri_T) as:

$$Ri_T = \frac{g\,r\,\beta(T - T_0)}{u_0^2}, \tag{S25}$$

where T is the bulk temperature of the initial eruption mixture, T_0 is the ambient atmospheric temperature, and $\beta = \frac{1}{T}$ is the thermal expansion coefficient. Thermal Richardson results are shown as $\frac{Ri_T}{\alpha}$ in Figure S7b.

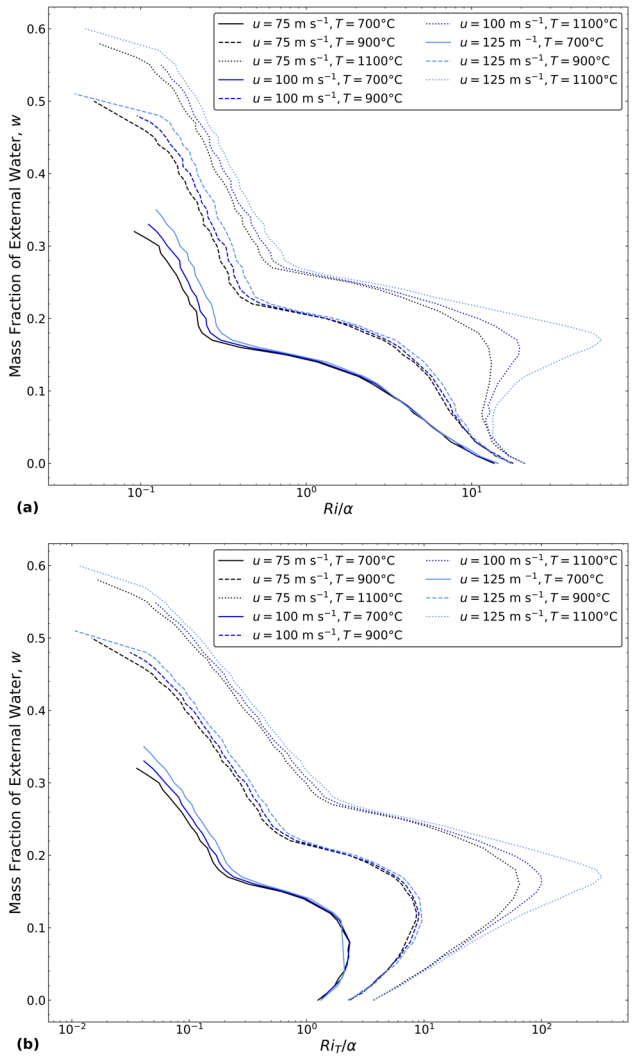

Figure S7: Depiction of the non-dimensional column collapse condition, illustrating where a buoyant plume can form as external water is added to the initial bulk mixture. This visualization is based on the thresholds presented in Figure 2 of the main text. Panel (a) shows the Richardson number divided by the entrainment coefficient (Ri/α), while panel (b) presents the Thermal Richardson number divided by the entrainment coefficient Ri_T/α, allowing for a direct comparison of these two parameters under varying conditions.

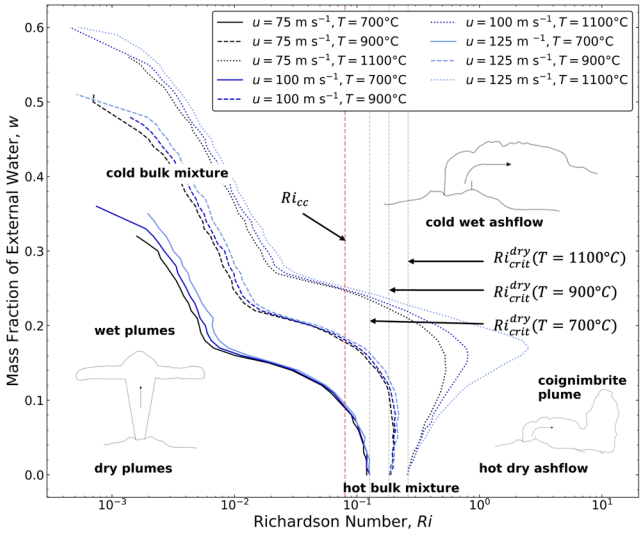

Figure S8: Depiction of the non-dimensional column collapse condition, illustrating where a buoyant plume can form as external water is added to the initial bulk mixture. This depiction is based on thresholds presented in Figure 2 of the main text. The red dashed line represents the analytical results calculated using Equation 5 from Koyaguchi and Suzuki [2018], while the black dashed lines correspond to the simulation results. Both Ri_{cc} (analytical) and Ri^{dry}_{crit} (simulation) are shown for the dry eruption case ($w = 0$). The figure also highlights the evolution of the Richardson number at the critical collapse condition as external water is introduced, demonstrating the contrast with the dry critical Richardson numbers (Ri_{cc} and Ri^{dry}_{crit}).

S9.3 Richardson number results comparison

Both Ri and Ri_T predict consistent thresholds for plume buoyancy and column collapse, regardless of whether Ri, Ri_T, or the modified formulation $\gamma = \frac{Ri}{\alpha}$ is used. This consistency, demonstrated in Figure S7a,b (and Figure 4b in the main text), highlights the robustness of these formulations in predicting column stability.

S9.4 Critical Richardson number for column collapse

We present the results from Figure 4b in the main text alongside the critical Richardson number for the column collapse condition (Figure S8), as outlined by Koyaguchi and Suzuki [2018] and Suzuki and Koyaguchi [2012]. Specifically, we use Equation 5 from Koyaguchi and Suzuki [2018] for the dry eruption case ($w = 0$), where Ri_{cc} represents the analytical results. For the simulation results, we define the Ri value for $w = 0$ as Ri^{dry}_{crit}. The critical Richardson number, (Ri_{cc}), is calculated assuming an initial velocity of 100 m s^{-1}, and only the results for an initial magma temperature of 900 °C are shown. Figure S8 provides a direct comparison of the Richardson number at the column collapse condition under analytical and numerical approaches. Furthermore, it allows for a clearer examination of the evolution of the critical Ri values for wet eruptions in relation to their dry eruption counterparts.

S10 Data sources and uncertainty calculations

The column height and mass eruption rate (MER) data presented in Figure 1 from the main text (excluding the Hunga 2022 eruption) were sourced from the Independent Volcanic Eruption Source Parameter Archive (IVESPA, version 1.0) [Aubry et al. 2021]. Uncertainty values for the MER were calculated using the method outlined in the supplementary information (SI-S01) of Aubry et al. [2023].

For the Hunga 2022 eruption, plume height values were obtained from Proud et al. [2022], while MER values were taken from Van Eaton et al. [2023]. The plotted plume height represents the average of the values reported by Proud et al. [2022]

and Carr et al. [2022], with uncertainty reflecting the range between these values. The MER for the Hunga 2022 eruption was plotted as the average of the range of values provided in the supplementary information of Van Eaton et al. [2023]. It should be noted, however, that this MER was calculated using the growth rate of the umbrella cloud, assuming a constant volumetric flow rate of particles, magmatic gas, and vaporized seawater. Recent studies, however, suggest that this estimate may be too high [Mastin et al. 2024]. This is largely attributed to the vapor-rich nature of the Hunga plume, which indicates that most of the erupted tephra likely settled into pyroclastic flows rather than being carried upwards into the plume.

Copyright notice

References

Aubry, T. J., S. Engwell, C. Bonadonna, G. Carazzo, S. Scollo, A. R. Van Eaton, I. A. Taylor, D. Jessop, J. Eychenne, M. Gouhier, L. G. Mastin, K. L. Wallace, S. Biass, M. Bursik, R. G. Grainger, A. M. Jellinek, and A. Schmidt (2021). "The Independent Volcanic Eruption Source Parameter Archive (IVESPA, version 1.0): A new observational database to support explosive eruptive column model validation and development". In: *Journal of Volcanology and Geothermal Research* 417, page 107295. DOI: https://doi.org/10.1016/j.jvolgeores.2021.107295.

Aubry, T. J., S. L. Engwell, C. Bonadonna, L. G. Mastin, G. Carazzo, A. R. Van Eaton, D. E. Jessop, R. G. Grainger, S. Scollo, I. A. Taylor, A. M. Jellinek, A. Schmidt, S. Biass, and M. Gouhier (2023). "New Insights Into the Relationship Between Mass Eruption Rate and Volcanic Column Height Based On the IVESPA Data Set". In: *Geophysical Research Letters* 50(14), e2022GL102633. DOI: https://doi.org/10.1029/2022GL102633.

Carr, J. L., Á. Horváth, D. L. Wu, and M. D. Friberg (2022). "Stereo Plume Height and Motion Retrievals for the Record-Setting Hunga Tonga-Hunga Ha'apai Eruption of 15 January 2022". In: *Geophysical Research Letters* 49(9). DOI: https://doi.org/10.1029/2022GL098131.

Degruyter, W. and C. Bonadonna (2012). "Improving on mass flow rate estimates of volcanic eruptions". In: *Geophysical Research Letters* 39(16). DOI: https://doi.org/10.1029/2012GL052566.

Gupta, A. K., R. Bennartz, K. E. Fauria, and T. Mittal (2022). "Eruption chronology of the December 2021 to January 2022 Hunga Tonga-Hunga Ha'apai eruption sequence". In: *Communications Earth & Environment* 3(1), pages 1–10. DOI: https://doi.org/10.1038/s43247-022-00606-3.

Koyaguchi, T. and Y. J. Suzuki (2018). "The Condition of Eruption Column Collapse: 1. A Reference Model Based on Analytical Solutions". In: *Journal of Geophysical Research: Solid Earth* 123(9), pages 7461–7482. DOI: https://doi.org/10.1029/2017JB015308.

Koyaguchi, T. and A. W. Woods (1996). "On the formation of eruption columns following explosive mixing of magma and surface-water". In: *Journal of Geophysical Research* 101(B3), pages 5561–5574. DOI: https://doi.org/10.1029/95JB01687.

Mastin, L. G., A. R. Van Eaton, and S. J. Cronin (2024). "Did steam boost the height and growth rate of the giant Hunga eruption plume?" In: *Bulletin of Volcanology* 86(64). DOI: https://doi.org/10.1007/s00445-024-01749-1.

Mastin, L. G. (2007). "A user-friendly one-dimensional model for wet volcanic plumes". In: *Geochemistry, Geophysics, Geosystems* 8(3). DOI: 10.1029/2006GC001455.

– (2014). "Testing the accuracy of a 1-D volcanic plume model in estimating mass eruption rate". In: *Journal of Geophysical Research: Atmospheres* 119(5), pages 2474–2495. DOI: https://doi.org/10.1002/2013JD020604.

Mastin, L. G., M. Guffanti, R. Servranckx, P. Webley, S. Barsotti, K. Dean, A. Durant, J. Ewert, A. Neri, W. Rose, D. Schneider, L. Siebert, B. Stunder, G. Swanson, A. Tupper, A. Volentik, and C. Waythomas (2009). "A multidisciplinary effort to assign realistic source parameters to models of volcanic ash-cloud transport and dispersion during eruptions". In: *Journal of Volcanology and Geothermal Research* 186(1), pages 10–21. DOI: https://doi.org/10.1016/j.jvolgeores.2009.01.008.

Morton, B. R., G. Taylor, F. R. S, and J. S. Turner (1956). "Turbulent gravitational convection from maintained and instantaneous sources". In: *Proceedings of the Royal Society of London. Series A. Mathematical and Physical Sciences* 234(1196), pages 1–23. DOI: https://doi.org/10.1098/rspa.1956.0011.

Proud, S. R., A. T. Prata, and S. Schmauss (2022). "The January 2022 eruption of Hunga Tonga-Hunga Ha'apai volcano reached the mesosphere". In: *Science* 378(6619), pages 554–557. DOI: 10.1126/science.abo4076.

Rowell, C. R., A. M. Jellinek, S. Hajimirza, and T. J. Aubry (2022). "External Surface Water Influence on Explosive Eruption Dynamics, With Implications for Stratospheric Sulfur Delivery and Volcano-Climate Feedback". In: *Frontiers in Earth Science* 10. DOI: 10.3389/feart.2022.788294.

Sparks, R., M. Bursik, S. Carey, J. Gilbert, L. Glaze, H. Sigurdsson, and A. Woods (1997). *Volcanic plumes*. Wiley, pages 100–120. ISBN: 0471939013.

Suzuki, Y. J. and T. Koyaguchi (2012). "3-D numerical simulations of eruption column collapse: Effects of vent size on pressure-balanced jet/plumes". In: *Journal of Volcanology and Geothermal Research* 221-222, pages 1–13. DOI: https://doi.org/10.1016/j.jvolgeores.2012.01.013.

Van Eaton, A. R., J. Lapierre, S. A. Behnke, C. Vagasky, C. J. Schultz, M. Pavolonis, K. Bedka, and K. Khlopenkov (2023). "Lightning Rings and Gravity Waves: Insights Into the Giant Eruption Plume From Tonga's Hunga Volcano on 15 January 2022". In: *Geophysical Research Letters* 50(12). DOI: https://doi.org/10.1029/2022GL102341.

Wohletz, K. H. (1986). "Explosive magma-water interactions: Thermodynamics, explosion mechanisms, and field studies". In: *Bulletin of Volcanology* 48, pages 245–264. DOI: https://doi.org/10.1007/BF01081754.

Woods, A. (1993). "Moist convection and the injection of volcanic ash into the atmosphere". In: *Journal of Geophysical Research: Solid Earth* 98(B10), page 17. DOI: https://doi.org/10.1029/93jb00718.